Journal of Power Sources 268 (2014) 596–603

Contents lists available at ScienceDirect

Journal of Power Sources

journal homepage: www.elsevier.com/locate/jpowsour

Mechanism and kinetics of sodium borohydride hydrolysis over crystalline nickel and nickel boride and amorphous nickel–boron nanoparticles

Zhijie Wu [a, c, *], Xikang Mao [a], Qin Zi [a], Rongrong Zhang [a], Tao Dou [a], Alex C.K. Yip [b, **]

[a] State Key Laboratory of Heavy Oil Processing and the Key Laboratory of Catalysis of CNPC, China University of Petroleum, Beijing 102249, China
[b] Department of Chemical and Process Engineering, University of Canterbury, Christchurch, New Zealand
[c] Key Laboratory of Advanced Energy Materials Chemistry (Ministry of Education), Collaborative Innovation Center of Chemical Science and Engineering (Tianjin), College of Chemistry, Nankai University, Tianjin 300071, China

HIGHLIGHTS

- A reaction route to describe borohydride hydrolysis over nickel catalysts.
- Presence of boron in nickel catalyst change hydrolysis routes.
- Nickel catalysts containing boron possess good hydrolysis activity.

GRAPHICAL ABSTRACT

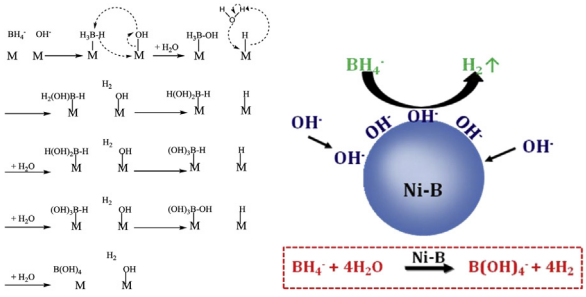

ARTICLE INFO

Article history:
Received 25 February 2014
Received in revised form
11 June 2014
Accepted 12 June 2014
Available online 20 June 2014

Keywords:
Borohydride
Hydrolysis
Hydrogen
Nickel catalyst
Amorphous nickel–boron nanoparticles

ABSTRACT

The initial hydrogen generation turnover rates during the hydrolysis of sodium borohydride over nickel catalysts (crystalline nickel (Ni), crystalline nickel boride (Ni_3B), and amorphous nickel–boron (Ni–B) nanoparticles) were measured to investigate the reaction kinetics and mechanisms by varying the reactant concentrations and reaction temperatures. Nickel catalysts with and without boron follow different hydrolysis pathways; hydroxide ions are involved in the activation of reactant molecules over Ni_3B and Ni–B catalysts. This study explicitly reports the zero-order and first-order reaction kinetics with respect to the reactant concentration over Ni, Ni_3B and Ni–B catalysts. The initial hydrogen generation turnover rates and activation energies determined from the experimental data indicate that the amorphous Ni–B nanoparticles exhibit the highest turnover rate and lowest activation energy for the hydrolysis of borohydride among the investigated catalysts. This study provides a general strategy for the development of borohydride hydrolysis catalysts via the modification of a metal catalyst using boron, which causes the crystalline structure to become amorphous and leads to electron-rich, highly undercoordinated metal atoms at the surface.

© 2014 Elsevier B.V. All rights reserved.

1. Introduction

Hydride salts such as sodium borohydride ($NaBH_4$) can be used as safe hydrogen reservoirs for the polymer electrolyte membrane fuel cells [1,2]. In general, metal, bimetallic or metal-boron catalysts

* Corresponding author. State Key Laboratory of Heavy Oil Processing and the Key Laboratory of Catalysis of CNPC, China University of Petroleum, Beijing 102249, China. Tel.: +86 10 8973 3235; fax: +86 10 8973 4979.
** Corresponding author.
E-mail addresses: zhijiewu@cup.edu.cn, zhijie.wu@hotmail.com (Z. Wu), alex.yip@canterbury.ac.nz (A.C.K. Yip).

http://dx.doi.org/10.1016/j.jpowsour.2014.06.067
0378-7753/© 2014 Elsevier B.V. All rights reserved.

are used to hydrolyse sodium borohydride and then generate hydrogen in a controlled manner [2–6]. To design and synthesise hydrolysis catalysts that possess high activity under high borohydride concentrations and low temperatures, the reaction mechanisms/pathways must be understood. Extensive studies of borohydride hydrolysis pathways and kinetics have been performed using novel metal and metal-boron catalysts [5–9]. Nevertheless, the effect of the reactant concentration on the hydrogen generation rate is difficult to ascertain based on the kinetics of the proposed pathways [3,10–19] because of a lack of information regarding the kinetically relevant steps [5–9,10].

The hydrolysis of sodium borohydride over Ru catalysts is generally hypothesised to be a first-order reaction with respect to the reactant concentration, whereas this hydrolysis catalysed by transition metals (Ni, Co, Fe) has been reported to be a zero-order reaction [1,5–19]. These first- and zero-order dependences can be explained by the Langmuir–Hinshelwood model for the single-site adsorption of BH_4^- onto the catalyst [1,14]. However, these previous kinetic studies did not consider the effect of the hydroxide ion concentrations on the reaction rates. For example, amorphous nickel–boron (Ni–B) and cobalt–boron (Co–B) catalysts exhibit high hydrogen generation rates in alkaline borohydride solutions with high hydroxide ion concentrations or low borohydride concentrations, whereas Ru catalysts exhibit high hydrogen generation rates under the opposite conditions [5–18]. These results indicate that hydroxide ions play a crucial role in the hydrolysis of borohydride on catalyst surfaces. In our previous work, we proposed that hydroxide ions substitute the hydrogen in BH_4^- to form $BH_{4-y}^-(OH^-)_y$ ($y = 1, 2, 3, 4$) [18]. To further validate this proposed mechanism, the kinetic relevance of the elementary steps and the effects of the metal species (crystalline nickel (Ni), crystalline nickel boride (Ni_3B), or amorphous nickel–boron (Ni–B)) on the initial hydrogen generation turnover rates during the hydrolysis of borohydride were examined by varying the reactant concentrations.

Herein, we report the intrinsic hydrolysis activities (denoted as the initial hydrogen generation turnover rates) of crystalline Ni and Ni_3B and of amorphous Ni–B clusters in the hydrolysis of sodium borohydride. We aim to provide a mechanistic interpretation of the kinetic data and to contrast the behaviour of a Ni metal surface with that of a Ni metal surface containing B atoms. Although the hydrolysis of borohydride over transition metals (Ni, Fe and Co) has been reported to be a zero-order reaction with respect to the borohydride concentrations [8,17], our recent studies [18] and some other reports [10–17] have shown that, when amorphous Ni/Co/Fe–boron nanoparticle catalysts are employed, the hydrolysis of borohydride is a first-order reaction with respect to the borohydride concentration and proceeds via different reaction intermediates on the surfaces of the metal-boron catalyst. We hypothesize that the different intermediates formed over different active sites (i.e., Ni, Ni_3B and Ni–B) under the same reaction conditions can explain this interesting kinetic behaviour. Based on the work of Peña-Alonso et al. [1], Guella et al. [5,6] and Holbrook et al. [8], we propose herein a modified hydrogen generation mechanism that involves hydroxide ions for the hydrolysis of borohydride over Ni–B catalysts, as illustrated in Fig. 1. First, borohydride and hydroxide ions in the solution are chemisorbed to the metal atoms. A proton on the borohydride ion then exchanges with a hydroxide ion to form M–H, which can further react with water to generate hydrogen gas. We attribute the different kinetic behaviours of metal and metal-boron nanoparticles during borohydride hydrolysis to the differences in the reaction pathways that occur at their surfaces. These behaviours on metal-boron catalysts are consistent irrespective of the boron contents and particle sizes.

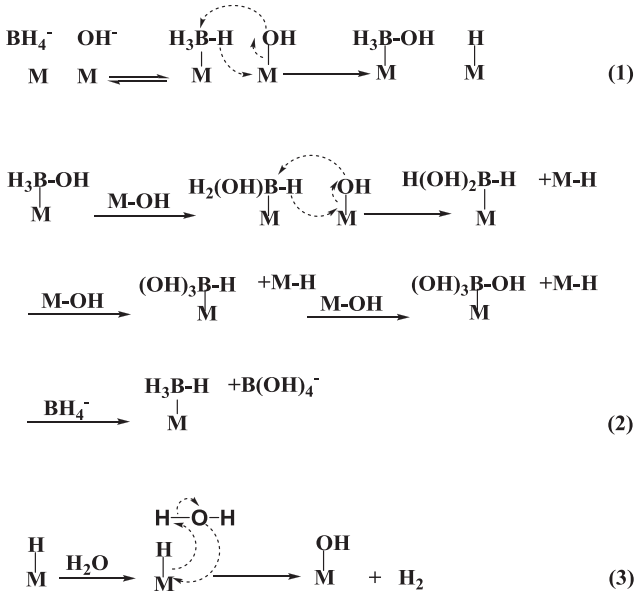

Fig. 1. The proposed mechanism for catalytic hydrogen production via hydrolysis from an aqueous borohydride solution.

2. Experimental

2.1. Materials

$NaBH_4$ (98%) and ethylenediamine (99.9%) were purchased from J&K Scientific, Ltd. (China). Nickel chloride (99.99%), nickel sulphate (99.99%), ethanol (99.99%), tetraethylene glycol (99%), $N_2H_4 \cdot H_2O$ (80 wt. %) and KBH_4 (98%) were purchased from Guanfu Chemical, Ltd. (Tianjin, China) and were used as received. The catalyst synthesis procedures described in Refs. [19–22] were used to prepare the Ni, Ni_3B, Ni–B-1 and Ni–B-2 catalysts, respectively.

Ni catalyst [19]: 2.1 g of nickel chloride was dissolved in 30.0 mL of ethanol, and then 10.0 g of an 80 wt.% $N_2H_4 \cdot H_2O$ solution and 10.0 mL of a 25 mol L^{-1} NaOH aqueous solution were added under stirring (800 rpm). The reaction was continued for several hours under stirring until bubbles were no longer released at room temperature. The obtained black nano-nickel catalyst was washed with distilled water until reaching a pH of 7, then washed five times with ethanol to remove the water and finally stored in ethanol.

Ni_3B catalyst [20]: 0.12 g of nickel chloride was dissolved in 15.0 mL of tetraethylene glycol (TEG) under ultrasonication for 10 min, and then the mixture was stirred (800 rpm) at 318 K under an Ar purge for 60 min. Subsequently, 15 mL of a previously freshly prepared and chilled solution of TEG and 0.50 g of KBH_4 were added dropwise (0.05 mL s^{-1}) to the metal salt solution. With continuous stirring under an Ar purge, the temperature was slowly ramped to 553 K and held for 5 min. Then, the reaction solution was cooled to room temperature, and the precipitates were collected by centrifugation, washed five times with ethanol, and dried under vacuum at 313 K for 12 h.

Ni–B-1 with a Ni/B molar ratio of 2 [21]: 11.1 mL of ethylenediamine was dissolved in 1800.0 mL of deionised water, and then 11.8 g of nickel chloride and 9.0 g of KBH_4 were added to the aqueous ethylenediamine solution under stirring (800 rpm), respectively. The pH of the solution was adjusted to 12.5–13.0 through the addition of 0.1 mol L^{-1} NaOH. To prepare amorphous Ni–B-1 nanoparticles, the solution was heated to 313 K. The reaction was continued until no bubbles were observed, and the resulting black solid was washed with distilled water until pH = 7,

and then washed five times with ethanol to remove the water. The solid was stored in ethanol.

Ni–B-2 with a Ni/B molar ratio of 3 [22]: 200 mL of 0.1 mol L^{-1} nickel chloride solution was placed in a three-necked flask immersed in an ice-salt bath (273 K). Under vigorous stirring, 50 mL of a 0.35 mol L^{-1} KBH_4 solution was added to the nickel chloride solution through a constant-flow pump (dropwise at a rate of 0.10 mL s^{-1}). The reaction was continued until no bubbles were observed after the addition of a KBH_4 solution, and the resulting black solid was washed with distilled water until reaching a pH of 7, then washed five times with ethanol to remove the water. The solid was stored in ethanol.

2.2. Characterization

Powder X-ray diffraction (XRD) patterns of the catalysts were obtained over a 2θ range of 30–80° at a scan rate of 4° min^{-1} on a Rigaku *D*/max 2500 X-ray diffractometer (Cu Kα, $\lambda = 1.54178$ Å) operated at 40 kV and 40 mA. The compositions of the samples were determined through inductively coupled plasma atomic emission spectrometry (ICPAES) using an IRIS Intrepid spectrometer. The morphology and particle size were examined via transmission electron microscopy (TEM) using a FEI Tecnai G2 high-resolution transmission electron microscope operated at 200 kV. Samples were mounted by dispersing on ethanol on a lacey carbon Formvar coated Cu grid. The X-ray photoelectron spectroscopy (XPS) of the catalysts were recorded with a Kratos Axis Ultra DLD spectrometer equipped with a monochromatic Al Kα source, hybrid magnetic/electrostatic optics, and a multichannel plate and delay line detector.

Chemisorption experiments were performed using a pulse chromatographic microreactor [21]. Approximately 200 mg of catalyst was treated at 573 K (ramping rate of 0.083 K s^{-1}) under flowing Ar gas (1.67 mL s^{-1}) for 2 h. The sample was then cooled to 303 K, and 1% H_2 in Ar was injected every 5 min until the calculated areas of the consecutive pulses became constant. The dispersion of Ni was calculated by assuming a $H/Ni_{(surf)}$ ratio of 1 and a surface area of 6.5×10^{-20} m^2 per Ni atom [21].

2.3. Hydrolysis reactions

The hydrolysis reaction was performed in a small glass reactor (200 mL) in a bath-type hydrogen generator [15]. A typical measurement consisted of introducing the catalyst (0.0050–0.20 g) into the reactor along with a solution containing $NaBH_4$ and NaOH. The outgoing hydrogen stream was then passed through silica gel to remove any moisture. The hydrogen generation rate (mL min^{-1}) was measured using a hydrogen flow meter (CS2000, Beijing Sevenstar Electronics Co., Ltd.). The initial hydrogen generation rate was recorded, and the initial hydrogen generation turnover rate (per surface metal atom, as determined from the chemisorption uptake) was calculated (mol_{H2} $mol^{-1}_{surf\text{-}metal}$ s^{-1}). The amounts of borohydride and catalyst (weight ratio of 10–500) were chosen to ensure that the initial hydrogen generation turnover rates were recorded far from the reaction equilibrium.

The mass-transfer limitations during the reaction were investigated using procedures described elsewhere [23]. The experiments were performed using a stirring speed of 500 rpm to exclude external mass-transfer limitations. Intraparticle (internal) mass-transfer limitations were eliminated by sonicating the catalysts, which were dispersed in 5.0 mL of an aqueous solution for 10–30 min. The treated catalysts were tested under the same reaction conditions used for the untreated catalysts. The hydrogen generation rates of the treated catalysts were comparable to those of the untreated catalysts. Hence, no internal mass-transfer limitations were observed under the reaction conditions employed in this work.

2.4. Data analysis method

The borohydride hydrolysis mechanisms and the derivations of the analytical expressions for the reaction rates, the activation energies and the reaction orders were proposed based on heterogeneous catalytic reaction kinetics [24,25]. The following assumptions were used in all of the formulations:

(1) The adsorption follows the Langmuir equation, and the reactions obey Langmuir–Hinshelwood or Eley–Rideal reaction mechanisms.
(2) The elementary reactions are microscopically reversible.
(3) All active sites are identical, and the number of active sites is constant under all reaction conditions.
(4) Each intermediate adsorbs onto one active site, and the intermediates do not interact with each other.

3. Results and discussion

3.1. Catalyst properties

The atomic compositions of the crystalline Ni and Ni_3B nanoparticles and of the amorphous Ni–B-1 and Ni–B-2 nanoparticles are listed in Table 1. The Ni–B-1 ($Ni_{67.4}B_{32.6}$, Ni_2B) has a higher boron content than crystalline Ni_3B, whereas Ni–B-2 ($Ni_{74.5}B_{25.5}$, Ni_3B) has a composition similar to that of crystalline Ni_3B. Fig. 2 shows the XRD patterns of the Ni and Ni_3B as well as of the Ni–B-1 and Ni–B-2 nanoparticles. The XRD patterns of the Ni nanoparticles have three reflection peaks at $2\theta = 44.6°$, 51.9° and 76.2°, which correspond to the Ni(111), (200) and (220) lattice planes, respectively; these results indicate that the metallic nickel particles have the face-centred-cubic structure. The XRD patterns of the Ni_3B samples only contain peaks characteristic of Ni_3B compounds (JCPDS No. 17-0335), whereas those of the Ni–B nanoparticles contain a broad, featureless peak at $2\theta \approx 45°$ because of their amorphous structure. These data indicate that crystalline Ni and Ni_3B and amorphous Ni–B nanoparticles were successfully synthesized.

The TEM images (Fig. 3) show that the Ni and Ni_3B nanoparticles are ~40 nm quasi spheres. The Ni–B-1 nanoparticles are ~30 nm in diameter and exhibit a spherical, flower-like morphology, which is consistent with our previous results [19,21]. In contrast, the Ni–B-2 nanoparticles are ~40 nm in diameter and exhibit a solid, spherical morphology. Ni–B-1 possesses the smallest particle size, suggesting the highest surface to bulk atomic ratio (hence the surface concentration of active sites per gram of catalyst) in agreement with the hydrogen chemisorption results. The hydrogen chemisorption results indicate a low metal dispersion of 0.020, 0.011, 0.025, and 0.012 for Ni, Ni_3B, Ni–B-1 and Ni–B-2, respectively, and suggest that the Ni–B-1 particles have the largest active metal surface area (Table 1).

As indicated by the XPS analyses, the Ni 2p 3/2 binding energies of Ni–B-1 and Ni–B-2 are slightly lower than those of Ni (Table 1) because of electron transfer from boron to nickel [21]. These results indicate that the amorphous Ni–B nanoparticles have a different structure and different surface electron properties than those of crystalline Ni. In particular, amorphous Ni–B exhibits the characteristics of electron-rich, highly undercoordinated nickel atoms [19,21–23,26–30].

Amorphous Ni–B nanoparticles show superior catalytic properties (activity, selectivity and stability) in hydrogenation compared to their crystalline counterparts because of their unique isotropic

Table 1
Properties of the Ni, Ni_3B and Ni–B catalysts.[a]

Catalyst	Compositions (at. %)	Ni:B ratio (atom)	Amount of chemisorbed H_2 ($\mu mol\ g_{Ni}^{-1}$)	S_{Ni} ($m^2\ g^{-1}$)	Dispersion	Binding energies (eV)[b]	
						Ni 2p 3/2	B 1s
Ni	Ni	–	176	13.2	0.020	853.4,	–
Ni_3B	$Ni_{75.8}B_{24.2}$	3:1	94	7.3	0.011	853.0	187.6
Ni–B-1	$Ni_{67.4}B_{32.6}$	2:1	213	16.7	0.025	853.1	188.4
Ni–B-2	$Ni_{74.5}B_{25.5}$	3:1	99	7.8	0.012	853.1	188.2

[a] The amount of chemisorbed H_2, S_{Ni} and dispersion (D) were obtained from hydrogen chemisorptions. The dispersion (D) was calculated as $D = N_s/N_T$, assuming $H/Ni_{(surf)} = 1$ [36], where N_s and N_T are the numbers of surface atoms and total atoms, respectively. The relationship between the active nickel surface area (S_{Ni}) and dispersion (D) is given by $S_{Ni} = a_m \times (N_A/M) \times D$ [36], where a_m is the surface area per atom (6.51×10^{-20} m^2 per Ni atom), N_A is Avogadro's constant and M is the atomic mass.
[b] Ni and B binding energies determined from the XPS analysis.

structure and high concentration of coordinatively unsaturated metal sites [26–30]. Specifically, Ni–B nanoparticles with Ni/B molar ratios of 2 (Ni_2B) and 3 (Ni_3B) are frequently reported to be excellent catalysts [30]. Here, amorphous Ni–B-1 (Ni_2B) and Ni–B-2 (Ni_3B) nanoparticles were prepared and investigated using hydrogen generation experiments to elucidate the effects of the B content on the reaction kinetics and mechanisms, as discussed in the following section.

3.2. Hydrogen generation rates of nickel-based catalysts

Fig. 4a shows the initial hydrogen generation turnover rates for the different catalysts at 303 K as a function of the borohydride concentration. For all of the nickel catalysts, the initial hydrogen generation turnover rates increased as the borohydride concentration increased from 0.01 to 0.26 mol L^{-1}. The initial hydrogen generation rates over Ni_3B, Ni–B-1 and Ni–B-2 decreased linearly when the borohydride concentration further increased from 0.26 to 1.84 mol L^{-1} (Fig. 4c). In contrast, the initial hydrogen generation rate over the crystalline Ni catalyst remained unchanged (Fig. 4c). These results are consistent with first-order and zero-order reactions with respect to the borohydride concentration for the metal-boron and nickel metal catalysts, respectively [5–18].

The initial hydrogen generation turnover rates of Ni_3B, Ni–B-1 and Ni–B-2 exhibited similar trends as a function of the hydroxide ion concentration; the rates increased rapidly and then decreased at high hydroxide ion concentrations (Fig. 4b). In contrast to Ni_3B, Ni–B-1 and Ni–B-2, the initial hydrogen generation turnover rate of the Ni nanoparticles decreased monotonically as the hydroxide ion concentration increased; this result is consistent with Ru-catalysed hydrogen generation [10–18]. Our data demonstrate that hydroxide ions not only can enhance the hydrogen generation rates over boron-containing nickel catalysts but that they also clearly inhibit hydrogen generation over pure nickel catalysts. The different effects of the hydroxide ion concentration on these catalysts are commonly attributed to their different reaction mechanisms [5–18], which should involve the formation of different intermediates on their surfaces. Amorphous Ni–B is characterized by highly under-coordinated nickel atoms, and the Ni atoms are electron-rich because of electron transfer from boron [18,21,23,28–30]. These properties enable the efficient activation of unsaturated reactants (e.g., alkenes, aromatics, etc.). Moreover, the metal conductivity and hydrogen adsorption ability are altered by the presence of boron [26,27]. Therefore, amorphous Ni–B nanoparticles generally exhibit unique selectivity compared to nickel or Raney nickel catalysts in catalytic hydrogenation [28–30]. Here, the different effects of the borohydride and hydroxide ion concentrations on the activities of the nickel catalysts with and without boron can be attributed to different reaction intermediates. This is so because the activation of borohydride anions over Ni–B nanoparticles should be more difficult due to the presence of electron-rich Ni atoms [18,21,23] and because the hydrogen species on Ni–B nanoparticles should become active [26,27]. These data suggest that the borohydride hydrolysis pathways on nickel with and without boron differ, as described in the following section.

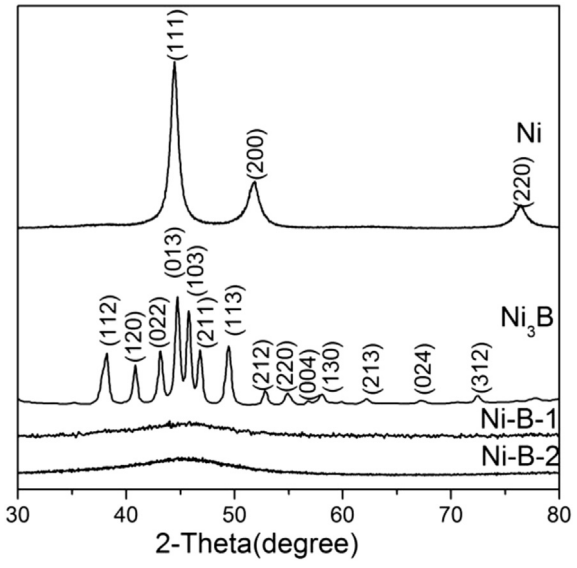

Fig. 2. XRD patterns of the Ni, Ni_3B, Ni–B-1 and Ni–B-2 nanoparticles.

3.3. Elementary steps for borohydride hydrolysis on Ni, Ni_3B and Ni–B nanoparticles

Based on previous work [1,5–9] and Figs. 1 and 5 presents the elementary steps for the hydrolysis of borohydride over the catalysts. The dissociative adsorption of BH_4^- anions should be more difficult on the surfaces of Ni–B nanoparticles than on the surfaces of pure metals [5–9] because of the presence of electron-rich Ni atoms. As shown in Fig. 5a, BH_4^- and OH^- adsorb onto the catalyst surface to form M–BH_4 and M–OH, which are the most abundant reactive intermediates, via quasi-equilibrated reactions. The quasi-equilibrium assumption requires rapid BH_4^- and OH^- adsorption–desorption processes at the time scale of the kinetically relevant molecular- or ion-adsorption events.

The surface coverages (θ_i, $i = BH_4^-, OH^-$) of the adsorbed species are given by the Langmuir adsorption isotherms for steps (1.1) and (1.2) without considering the adsorption of other species (e.g., $BH_y(OH)_{1-y}$, H_2O, H, etc.) [24,25]:

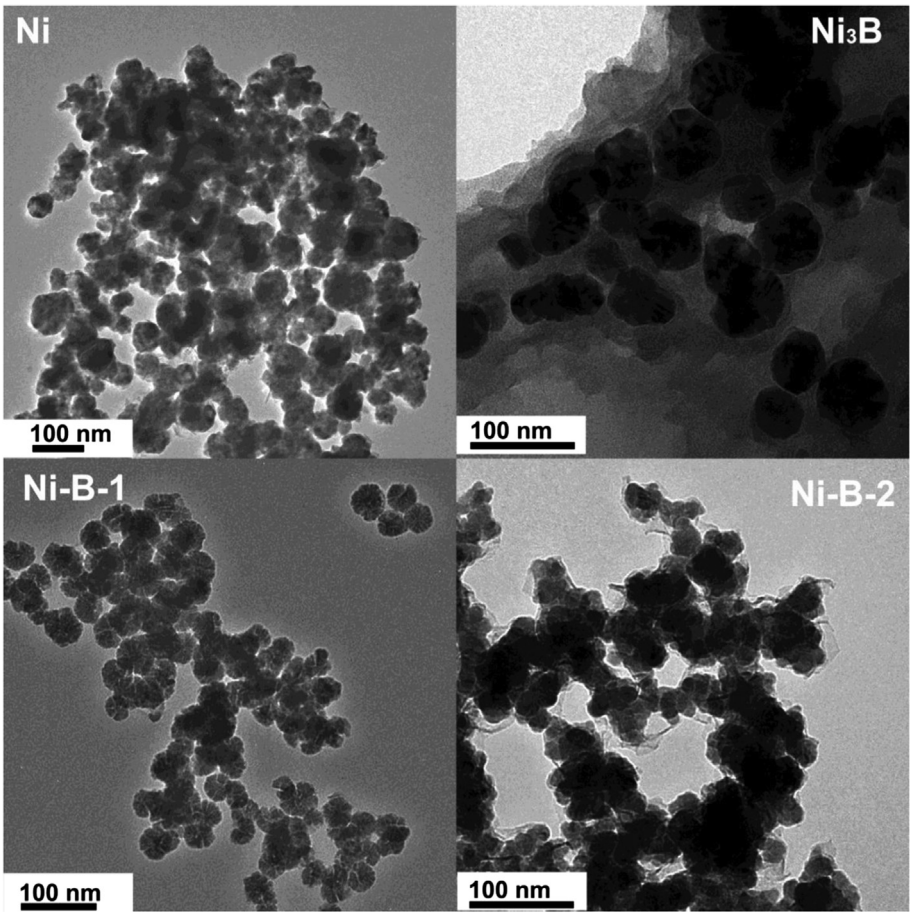

Fig. 3. TEM images of the Ni, Ni_3B, Ni–B-1 and Ni–B-2 nanoparticles.

$$\theta_{MBH_4} = \frac{K_{BH_4}\left[BH_4^-\right]}{1 + K_{BH_4}\left[BH_4^-\right] + K_{OH}\left[OH^-\right]} \quad (1)$$

$$\theta_{MOH} = \frac{K_{OH}\left[OH^-\right]}{1 + K_{BH_4}\left[BH_4^-\right] + K_{OH}\left[OH^-\right]} \quad (2)$$

Similar to borohydride activation, we hypothesize that hydroxide ion activation is also difficult because of the electron-rich Ni atoms at the Ni–B surface. Moreover, the hydrogen adsorbed onto the metal-boron nanoparticles should react with water to generate hydrogen gas (step (1.8)) [26,27,31]. Thus, step (1.3) was assumed to be the rate-determining step on the Ni_3B, Ni–B-1 and Ni–B-2 catalysts. The reaction turnover rate can then be written as:

$$r = k_1[MBH_4][MOH] = \frac{k_1 K_{BH_4}\left[BH_4^-\right] K_{OH}\left[OH^-\right]}{\left(1 + K_{BH_4}\left[BH_4^-\right] + K_{OH}\left[OH^-\right]\right)^2} \quad (3)$$

Under certain conditions, the rate can be simplified to:

$$r = \frac{k_1 K_{BH_4}\left[BH_4^-\right] K_{OH}\left[OH^-\right]}{\left(1 + K_{BH_4}\left[BH_4^-\right] + K_{OH}\left[OH^-\right]\right)^2} = \frac{\alpha}{\left[BH_4^-\right]} = \frac{\beta}{\left[OH^-\right]} \quad (4)$$

when

$$K_{BH_4}\left[BH_4^-\right] \gg 1 + K_{OH}\left[OH^-\right],\ \alpha = \frac{k_1 K_{OH}\left[OH^-\right]}{K_{BH_4}}.$$

when

$$K_{OH}\left[OH^-\right] \gg 1 + K_{BH_4}\left[BH_4^-\right],\ \beta = \frac{k_1 K_{BH_4}\left[BH_4^-\right]}{K_{OH}}.$$

Alternatively, the rate simplifies to:

$$r = \frac{k_1 K_{BH_4}\left[BH_4^-\right] K_{OH}\left[OH^-\right]}{\left(1 + K_{BH_4}\left[BH_4^-\right] + K_{OH}\left[OH^-\right]\right)^2} = \chi\left[BH_4^-\right] = \delta\left[OH^-\right] \quad (5)$$

when

$$K_{BH_4}\left[BH_4^-\right] + 1 \ll K_{OH}\left[OH^-\right],\ \chi = \frac{k_1 K_{BH_4}}{K_{OH^-}\left[OH^-\right]}.$$

when

$$K_{OH}\left[OH^-\right] + 1 \ll K_{BH_4}\left[BH_4^-\right],\ \delta = \frac{k_1 K_{OH^-}}{K_{BH_4^-}\left[BH_4^-\right]}.$$

Equation (4) suggests that the reaction rate increases with decreasing borohydride or hydroxide ion concentration under

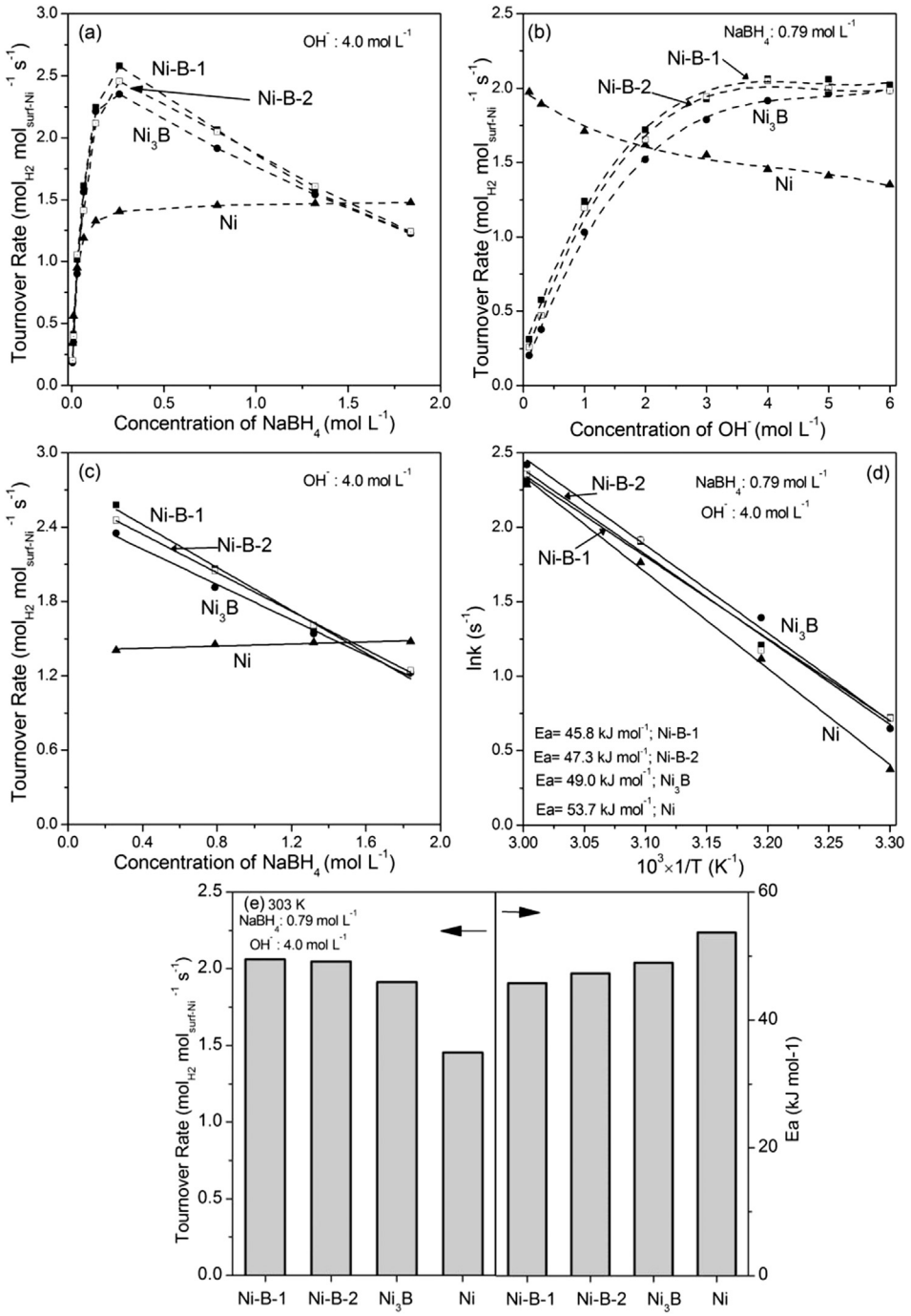

Fig. 4. Initial hydrogen generation rates for sodium borohydride hydrolysis over Ni, Ni_3B Ni–B-1, and Ni–B-2 catalysts at 303 K. (a) Effect of the borohydride concentration; (b) effect of the hydroxide concentration; (c) effect of the borohydride concentration; (d) the borohydride hydrolysis activation energies and (e) a comparison of the initial hydrogen generation turnover rates and activation energies.

specific reaction conditions. This rate expression is consistent with the rate data obtained from the hydrolysis of borohydride over Ni_3B, Ni–B-1 and Ni–B-2, as shown in Fig. 4b and c. Equation (5) indicates that the reaction rate increases rapidly as the borohydride or hydroxide ion concentration increases when their initial concentrations are low (Fig. 4a and b).

Both amorphous Ni–B nanoparticle catalysts (Ni–B-1 and Ni–B-2) exhibited almost identical kinetic behaviour, suggesting that the same hydrolysis pathways occurred irrespective of the boron content. However, Fig. 4a indicates slightly higher initial hydrogen generation turnover rates over Ni–B-1 than over Ni–B-2, suggesting that the boron content has an enhancing effect on activity, which is consistent with previous results [22].

To investigate the structure sensitivity of the borohydride hydrolysis, the effect of Ni–B nanoparticle size on the activity was also studied (Fig. S1). The initial hydrogen generation turnover rates (based on active surface sites) negligibly changed when the Ni–B particle size increased, suggesting that the reaction over amorphous Ni–B catalysts is insensitive to the structure of the catalysts. These results exclude the effect of catalyst size on the kinetic behaviour and reaction pathway for the hydrolysis of NaBH4. Thus, it is expected that reducing the particle size of Ni–B nanoparticles

(a)

$$BH_4^- + M \overset{K_{BH4}}{\rightleftharpoons} MBH_4 \quad (1.1)$$

$$M + OH^- \overset{K_{OH}}{\rightleftharpoons} MOH \quad (1.2)$$

$$MBH_4 + MOH \xrightarrow{k_1} MBH_3OH + MH \quad (1.3)$$

$$MBH_3OH + MOH \rightleftharpoons MBH_2(OH)_2 + MH \quad (1.4)$$

$$MBH_2(OH)_2 + MOH \rightleftharpoons MBH(OH)_3 + MH \quad (1.5)$$

$$MBH(OH)_3 + MOH \rightleftharpoons MB(OH)_4 + MH \quad (1.6)$$

$$MB(OH)_4 \rightleftharpoons B(OH)_4^- + M \quad (1.7)$$

$$MH + H_2O \xrightarrow{k_2} MOH + H_2 \quad (1.8)$$

(b)

$$BH_4^- + M + M \overset{K_{BH4}}{\rightleftharpoons} MBH_3 + MH \quad (2.1)$$

$$MBH_3 + H_2O \rightleftharpoons BH_3OH^- + MH \quad (2.2)$$

$$BH_3OH^- + M + M \rightleftharpoons MBH_2OH + MH \quad (2.3)$$

$$MBH_2OH + H_2O \rightleftharpoons BH_2(OH)_2^- + MH \quad (2.4)$$

$$BH_2(OH)_2^- + M + M \rightleftharpoons MBH(OH)_2 + MH \quad (2.5)$$

$$MBH(OH)_2 + H_2O \rightleftharpoons BH(OH)_3^- + MH \quad (2.6)$$

$$BH(OH)_3^- + M + M \rightleftharpoons MB(OH)_3 + MH \quad (2.7)$$

$$MB(OH)_3 + H_2O \rightleftharpoons B(OH)_4^- + MH \quad (2.8)$$

$$M + OH^- \overset{K_{OH}}{\rightleftharpoons} MOH \quad (2.9)$$

$$MH + MH \xrightarrow{k} 2M + H_2 \quad (2.10)$$

Fig. 5. Proposed reaction pathways for borohydride hydrolysis over (a) Ni_3B, Ni–B and (b) Ni catalysts. (M is a metal surface site, denotes a quasi-equilibrated step, and k_x and K_x are the kinetic and equilibrium constants, respectively, for the individual elementary steps).

has a positive effect on increasing the hydrogen generation rates if the rates are calculated based on the mass of catalysts (per gram of catalyst) because of the increase in the surface to bulk atomic ratio (hence the surface concentration of active sites per gram of catalyst) achieved by decreasing the particle sizes, in agreement with the literature [14,28–30].

For borohydride hydrolysis over metal surfaces, the dissociative adsorption of BH_4^- cations has been confirmed in previous studies [5–9]. A modified hydrolysis pathway is proposed in Fig. 5b. The surface coverages (θ_i, $i = BH_3^-$, H, OH^-, $B(OH)_4^-$, etc.) of the adsorbed species are given by the Langmuir adsorption isotherms from steps (2.1) and (2.2) without considering the adsorption of other species (e.g., $BH_y(OH)_{1-y}$, H_2O, etc.) [24,25]:

$$\theta_{MH} = \theta_{MBH_3} = \frac{\frac{K_{BH_4}^{1/2}[BH_4^-]^{1/2}}{(1+K_{OH}[OH^-])^{1/2}}}{1 + 2 \times \frac{K_{BH_4}^{1/2}[BH_4^-]^{1/2}}{(1+K_{OH}[OH^-])^{1/2}}} \quad (6)$$

Step (2.10) was assumed to be the rate-determining step based on previous studies [5–9]; thus, the reaction rate can be written as:

$$r = k[MH][MH] = \frac{kK_{BH_4}[BH_4^-]}{(1+K_{OH}[OH^-]) \times \left(1 + 2 \times \frac{K_{BH_4}^{1/2}[BH_4^-]^{1/2}}{(1+K_{OH}[OH^-])^{1/2}}\right)^2} \quad (7)$$

Under certain conditions, the rate simplifies to:

$$r = \frac{kK_{BH_4}[BH_4^-]}{(1+K_{OH}[OH^-]) \times \left(1 + 2 \times \frac{K_{BH_4}^{1/2}[BH_4^-]^{1/2}}{(1+K_{OH}[OH^-])^{1/2}}\right)^2} = \varepsilon[BH_4^-] = \frac{\eta}{[OH^-]} \quad (8)$$

when

$$K_{BH_4}[BH_4^-] \ll 1 + K_{OH}[OH^-],\ \varepsilon = \frac{kK_{BH_4}}{1 + K_{OH}[OH^-]}.$$

when

$$K_{BH_4}[BH_4^-] \ll 1 \ll K_{OH}[OH^-],\ \eta = \frac{kK_{BH_4}[BH_4^-]}{K_{OH}}.$$

The rate can also be expressed as:

$$r = \frac{kK_{BH_4}[BH_4^-]}{(1+K_{OH}[OH^-]) \times \left(1 + 2 \times \frac{K_{BH_4}^{1/2}[BH_4^-]^{1/2}}{(1+K_{OH}[OH^-])^{1/2}}\right)^2} = k' \quad (9)$$

where $k' = k/4 \times (1 + K_{OH}[OH^-])$ when $K_{BH_4}[BH_4^-] >> 1 + K_{OH}[OH^-] >> 1$.

Equation (8) suggests that the reaction rate increases with increasing borohydride or decreasing hydroxide ion concentration under specific reaction conditions (e.g., when the borohydride concentration is low, Fig. 4a and b), which was also observed by Mesmier et al. [32]. When the borohydride concentration is high, however, the rate is not affected by the reactant concentrations, as shown by Equation (9). This conclusion is consistent with the results obtained when a sodium borohydride concentration of 0.26–1.84 mol L^{-1} was used in the hydrolysis over the Ni catalyst (Fig. 4c) and with results reported in the literature [9,33].

On the basis of our proposed borohydride hydrolysis pathways shown in Fig. 5, new kinetic models can be formulated to explain the different kinetic behaviours reported for metal catalysts with and without boron [10–18]. However, the real hydrolysis pathways might be more complex under certain reaction conditions. For example, hydroxide ions greatly influence the solubility of borohydride, leading to the inhibition of hydrogen generation at high pH levels [10,34]. The present work demonstrates that the kinetic behaviour is highly dependent on the reactant and hydroxide ion concentrations because both species are involved in the hydrolysis. Additionally, the kinetic behaviour appears to be affected by the presence of B, irrespective of the type of nanoparticles used (crystalline Ni_3B or amorphous Ni–B).

3.4. Activation energies of the nickel catalysts

Fig. 4c shows that, within the concentration range from 0.26 to 1.84 mol L^{-1}, the hydrolysis of borohydride over Ni_3B, Ni–B-1 and

Ni–B-2 catalysts follows first-order reaction kinetics with respect to the reactant concentrations, whereas that over the Ni catalyst is zero-order with respect to the reactant concentrations. The slope of the Arrhenius plot (Fig. 4d) provides activation energies (Ea) of ~45 kJ mol^{-1} and ~47 kJ mol^{-1} for the Ni–B-1 and Ni–B-2 catalysts, which are similar to previously reported values [17,18]. Fig. 4e indicates that the Ni–B nanoparticles had the highest initial hydrogen generation turnover rates and the lowest activation energy among the tested catalysts during the hydrolysis of borohydride at 303 K (reactant concentration of 0.79 mol L^{-1}). These results suggest that amorphous Ni–B exhibits higher catalytic activity in borohydride hydrolysis than does crystalline Ni and that the activity is proportional to the content of boron. This result is similar to the results for other transition metal-boron nanoparticles, e.g., Fe–B, Co–B and Ni–Co–B, and their corresponding metal catalysts. However, amorphous metal-boron catalysts do not exhibit satisfactory stability because their surfaces can easily be covered with non-active boron oxides [10–25]. Instead, crystalline metal borides obtained via heat treatment of the corresponding amorphous metal-boron nanoparticles exhibit better hydrogen generation rates per gram of catalyst [24,35], which suggests that crystalline metal boride should be a suitable catalyst for the hydrolysis of borohydride in alkaline aqueous solutions.

The use of sodium borohydride for hydrogen generation is highly effective, but an important barrier to overcome in commercializing this technology is the current cost of sodium borohydride [37–39]. The key to lowering cost is to develop a technically feasible, energy efficient sodium borohydride synthesis process [39]. In the existing commercial process, the primary energy input is used to produce sodium metal, which is used in large quantities in the subsequent chemical process to yield sodium borohydride. At present, developing a low-cost and reliable process for generating sodium borohydride from sodium borates is attracting considerable attention [37–40]. Here, an alkaline aqueous system appears to be suitable for metal-boron catalysts, leading to sodium borates and sodium hydroxide by-products in the hydrolysis of sodium borohydride, in contrast to hydrolysis over pure metal (e.g., Ru) catalysts. Therefore, a strategy that recovers both sodium borates and sodium hydroxide is required when using metal-boron as a borohydride hydrolysis catalyst. For instance, sodium hydroxide electrolysis can be used to reduce the cost to produce sodium metal and can then be used for sodium borohydride regeneration [40].

4. Conclusions

Crystalline Ni and Ni_3B and amorphous Ni–B were prepared and used to hydrolyse sodium borohydride and generate hydrogen. The catalyst kinetics were measured and used to propose a modified hydrolysis pathway. The differences in the kinetic behaviours are attributed to the different reaction pathways for borohydride hydrolysis over nickel catalysts with and without boron. During hydrogen generation, hydroxide anions interact with borohydride molecules over the Ni_3B and Ni–B catalysts. The amorphous Ni–B nanoparticles exhibited the highest initial hydrogen generation turnover rate and lowest activation energy among the investigated catalysts during hydrolysis under the same conditions. This study presented the hydrolysis results for nickel-based catalysts; however, these results could also be applicable to other metal catalysts (e.g., Co, Fe, Ru and Pd) that adopt amorphous structures when they are doped with boron.

Acknowledgements

This work was supported by the Science Foundation of China University of Petroleum-Beijing (YJRC-2013-38), the NSF of China (21206192), and the Doctoral Program of Higher Education of China (20120007120010), the Open Project of Key Lab Adv Energy Mat Chem (Nankai Univ) (KLAEMC-OP201201).

Appendix A. Supplementary data

Supplementary data related to this article can be found at http://dx.doi.org/10.1016/j.jpowsour.2014.06.067.

References

[1] R. Peña-Alonso, A. Sicurelli, E. Callone, G. Carturan, R. Raj, J. Power Sources 165 (2007) 315–323.
[2] J.H. Kim, H. Lee, S.C. Han, H.S. Kim, M.S. Song, J.Y. Lee, Int. J. Hydrogen Energy 29 (2004) 263–267.
[3] J.C. Ingersoll, N. Mani, J.C. Thenmozhiyal, A. Muthaiah, J. Power Sources 173 (2007) 450–457.
[4] W. Ye, H. Zhang, D. Xu, L. Ma, B. Yi, J. Power Sources 164 (2007) 544–548.
[5] G. Guella, C. Zanchetta, B. Patton, A. Miotello, J. Phys. Chem. B 110 (2006) 17024–17033.
[6] G. Guella, B. Patton, A. Miotello, J. Phys. Chem. C 111 (2007) 18744–18750.
[7] V. Diakov, M. Diwan, E. Shafirovich, A. Varma, Chem. Eng. Sci. 62 (2007) 5586–5591.
[8] K.A. Holbrook, P.J. Twist, J. Chem. Soc. A 6 (1971) 890–894.
[9] C.M. Kaufman, B. Sen, J. Chem. Soc. Dalton Trans. 14 (1985) 307–313.
[10] H. Dong, H. Yang, X. Ai, C. Cha, Int. J. Hydrogen Energy 28 (2003) 1095–1100.
[11] S.C. Amendola, S.L. Sharp-Goldman, M.S. Janjua, N.C. Spencer, M.T. Kelly, P.J. Petillo, M. Binder, Int. J. Hydrogen Energy 25 (2005) 969–975.
[12] B.H. Liu, Z.P. Li, S. Suda, J. Alloys Compd. 415 (2006) 288–293.
[13] S.U. Jeong, R.K. Kim, E.A. Cho, H.J. Kimb, S.W. Nam, I.H. Oh, S.A. Hong, S.H. Kim, J. Power Sources 144 (2005) 129–134.
[14] J.S. Zhang, W.N. Delgass, T.S. Fisher, J.P. Gore, J. Power Sources 164 (2007) 772–781.
[15] J.D. Ocon, T.N. Tuan, Y. Yi, R.L. de Leon, J.K. Lee, J. Lee, J. Power Sources 243 (2013) 444–450.
[16] J.A. Gardiner, J.W. Collat, J. Am. Chem. Soc. 87 (1964) 1692–1700.
[17] J.C. Walter, Kinetics of Catalyzed Sodium Borohydride Hydrolysis and Fuel Cell Applicability (Ph.D. Dissertation), Purdue University, 2007, ISBN 9780549303787.
[18] Z.J. Wu, S.H. Ge, Catal. Commun. 13 (2011) 40–43.
[19] Z.F. Zhao, Z.J. Wu, L.X. Zhou, M.H. Zhang, W. Li, K.Y. Tao, Catal. Commun. 9 (2008) 2191–2194.
[20] Z.L. Schaefer, X.L. Ke, P. Schiffer, R.E. Schaak, J. Phys. Chem. C 112 (2008) 19846–19851.
[21] Z.J. Wu, M.H. Zhang, Z.F. Zhao, W. Li, K.Y. Tao, J. Catal. 256 (2008) 323–330.
[22] H.X. Li, H. Li, W.L. Dai, M.H. Qiao, Appl. Catal. A 238 (2003) 119–130.
[23] S.H. Ge, Z.J. Wu, M.H. Zhang, W. Li, K.Y. Tao, Ind. Eng. Chem. Res. 45 (2006) 2229–2234.
[24] M. Boudart, G. Djéga-Mariadassou (Eds.), Kinetics of Heterogeneous Catalytic Reactions, Princeton University Press, 1984.
[25] H. Lynggaard, A. Andreasen, C. Stegelmann, P. Stoltze, Prog. Surf. Sci. 77 (2004) 71–137.
[26] M. Mitov, A. Popov, I. Dragieva, J. Appl. Electrochem. 29 (1999) 59–63.
[27] I.D. Dragieva, Z.B. Stoynov, K.J. Klabunde, Scr. Mater. 44 (2001) 2187–2191.
[28] Z.J. Wu, W. Li, M.H. Zhang, K.Y. Tao, Front. Chem. Eng. China 1 (2007) 87–95.
[29] Y. Pei, G.B. Zhou, N. Luan, B.N. Zong, M.H. Qiao, F. Tao, Chem. Soc. Rev. 41 (2012) 8140–8162.
[30] S. Carenco, D. Portehault, C. Boissière, N. Mézailles, C. Sanchez, Chem. Rev. 113 (2013) 7981–8065.
[31] R.C. Wade, D.G. Holah, A.N. Hughes, B.C. Hui, Catal. Rev. Sci. Eng. 14 (1976) 211–246.
[32] R.E. Mesmer, W.L. Jolly, Inorg. Chem. 1 (1962) 608–612.
[33] C.M. Kaufman, Catalytic Generation of Hydrogen from the Hydrolysis of Sodium-borohydride: Application in a Hydrogen/Oxygen Fuel Cell (Ph.D. Thesis), The Louisiana State University and Agricultural and Mechanical College, 1981.
[34] Y. Shang, R. Chen, Energy Fuel 20 (2006) 2142–2148.
[35] A.K. Figen, Int. J. Hydrogen Energy 38 (2013) 9186–9197.
[36] G. Bergeret, P. Gallezot, Particle Size, Dispersion Measurements, in: G. Ertl, H. Knozinger, F. Schuth, J. Weitkamp (Eds.), Handbook of Heterogeneous Catalysis, Wiley-VCH, 2008, pp. p738–765.
[37] Y.B. Tan, X.B. Yu, RSC Adv. 3 (2013) 23879–23894.
[38] T. Kemmitt, G.J. Gainsford, Int. J. Hydrogen Energy 34 (2009) 5726–5731.
[39] H.K. Atiyeh, B.R. Davis, Int. J. Hydrogen Energy 32 (2007) 229–236.
[40] M. T. Kelly, Patent, 2006, US 20060102489.